The electrical and optical properties of kesterites

JPhys Energy

PAPER

The electrical and optical properties of kesterites

Maarja Grossberg[1], Jüri Krustok[1,2], Charles J Hages[3], Douglas M Bishop[4], Oki Gunawan[4], Roland Scheer[5], Samantha M Lyam[5], Hannes Hempel[6], Sergiu Levcenco[6] and Thomas Unold[6]

[1] Department of Materials and Environmental Technology, Tallinn University of Technology, Ehitajate tee 5, 19086, Tallinn, Estonia
[2] Division of Physics, Tallinn University of Technology, Ehitajate tee 5, 19086, Tallinn, Estonia
[3] Department of Chemical Engineering, University of Florida, Gainesville, FL, 32611, United States of America
[4] IBM T.J. Watson Research Center, Yorktown Heights, NY 10598, United States of America
[5] Photovoltaics Group, Martin-Luther-University Halle-Wittenberg, D-06120 Halle (Saale), Germany
[6] Department Structure and Dynamics of Energy Materials, Helmholtz- Zentrum Berlin für Materialien and Energie GmbH, Hahn-Meitner Platz 1, D-14109 Berlin, Germany

E-mail: maarja.grossberg@taltech.ee

Keywords: kesterite, defects, carrier lifetime, doping density, carrier transport

Supplementary material for this article is available online

OPEN ACCESS

RECEIVED
12 April 2019

REVISED
5 June 2019

ACCEPTED FOR PUBLICATION
13 June 2019

PUBLISHED
21 August 2019

Abstract

Kesterite $Cu_2ZnSn(S_xSe_{1-x})_4$ (CZTSSe) semiconductor materials have been extensively studied over the past decade, however despite significant efforts, the open circuit voltage remains below 60% of the theoretical maximum. Understanding the optical and electrical properties is critical to explaining and solving the voltage deficit. This review aims to summarize the present knowledge of optical and electrical properties of kesterites and specifically focuses on experimental data of intrinsic defects, charge carrier density and transport, and minority carrier lifetime and related rate-limiting recombination mechanisms. It concludes with suggestions for further investigation of the electrical and optical properties of kesterite materials.

1. Introduction

The high interest in kesterite $Cu_2ZnSn(S_xSe_{1-x})_4$ (CZTSSe) absorber materials for thin film solar cells is a result of a high absorption coefficient of $\sim 10^4$ cm^{-1}, the opportunity for band gap tuning in the range of 1–1.5 eV, as well as from the earth-abundant and non-toxic nature of the constituent elements [1]. However, despite a growing research body, the open circuit voltage (V_{OC}) characteristics of the best kesterite solar cells remain at only 60% of the maximum achievable value under the terrestrial solar spectrum. Carrier recombination in the bulk and a high recombination rate at the absorber-buffer interface are considered as the main sources of the large V_{OC} deficit. The bulk recombination involves the extended band tail states, and deep intrinsic defect levels which result in strong non-radiative recombination evidenced by the low luminescence yield and short minority carrier lifetime in kesterite materials [2–5].

It is known, that CZTSSe crystallizes in the disordered kesterite structure, where the 2d -Wyckoff positions of the (001) cationic planes are randomly occupied by Cu and Zn atoms [6, 7]. While theoretical calculations by Chen *et al* [8] find the lowest formation energy for the kesterite crystal structure, cation disorder is present in CZTSSe due to the low energy difference between the stannite- and kesterite-related structures. It has been suggested that the Cu-Zn disorder in Cu_2ZnSnS_4 (CZTS) follows a second order phase transition with a critical temperature of ~260 °C for CZTS, which was first observed and introduced to describe the modifications in the Raman spectra of CZTS annealed at different temperatures [9]. A similar phenomenon has also been found in $Cu_2ZnSnSe_4$ (CZTSe), with a critical temperature of 200 °C [10], where the measured increase in band gap is explained by thermally induced ordering of Cu and Zn cations. While the remarkable effect of the order–disorder transition on the band gap and vibrational spectra is explained by Vineyard's theory [11], the disorder parameter itself is not experimentally determined in the probed samples. A recent direct comparison between resonant x-ray diffraction and photoluminescence (PL) data in CZTSe has confirmed a relationship between the Cu-Zn disorder and the band gap modification [12]. A change in the order parameter from 0 to 0.7 leads to a

significant increase in the band gap on the order of ~0.11 eV and ~0.20 eV for CZTSe and CZTS, respectively [10, 13].

The absorption coefficient for CZTS and CZTSe is about ~2–3 $\times$ 10^4 cm^{-1} at 1.6 eV and at 1.1 eV, respectively, as determined by the normal reflectance and transmittance [2, 13] spectroscopic ellipsometry (SE) [14–16] and external quantum efficiency [17] methods. In the recent review by Choi *et al* [18] the main theoretical and experimental results on the energy band structure and SE data were discussed and summarized. Recently, Zamulko *et al* [19] re-examined first principle theory at different levels in order to improve the description of the electronic structure and optical properties of CZTSSe. Nishiwaki *et al* [20] performed density functional calculation to study absorption band tail of the kesterites. In particular, a theoretical estimate for the tail energy of ~30 meV for both CZTS and CZTSe was obtained. It was suggested that quite large Urbach energies (~85 meV) observed in some experiments [13] could arise from the extensive cation disordering. However, unlike the band gap modifications, the band tailing of the absorption edge is not affected by Cu-Zn disorder at least for the probed range of the ordering parameter [2, 13, 21, 22]. The same applies also for the V_{OC} deficiency which is very insensitive to the Cu-Zn disorder [10, 21, 23].

Although hundreds of publications discuss the optical and electronic properties, which are essential to understand and solve the voltage deficit in kesterites, disagreement on carrier lifetimes, mobilities and the nature of the bandtails still exists. This report reviews the optical and electrical properties of kesterites based on a wide cross-section of experimental reports and is split into four sections. In the first part of this article, a review on the intrinsic defects in kesterites is given. The second part of the paper focuses on the determination of the minority carrier lifetime in kesterites and the rate-limiting recombination mechanism behind it. The third summarizes the present knowledge of the charge carrier transport in the kesterites. Finally, based on the critical overview of the current experimental data of the electrical and optical properties of kesterites that may limit continued device improvements, a summary of the state-of-knowledge on this topic is given.

2. Intrinsic defects in kesterites

Experimental and theoretical studies of kesterites have identified intrinsic point defects and associated band tailing as the key limiting factors behind the large V_{OC} deficit [3, 24–26]. PL and admittance spectroscopy (AS) are the most used experimental methods to study defects in kesterites. PL studies have shown that most of the kesterite materials show properties that are typical for highly doped and compensated semiconductors [2, 5, 27–29]. In kesterites, the high doping originates from the very high concentration of charged intrinsic defects ($>10^{20}$ cm^{-1}) that cause widening of the defect levels within the forbidden gap and induce the spatial potential fluctuations and formation of band tails. In a p-type material and in the case of a small effective mass for electrons, like in kesterites, radiative recombination can mainly arise from four different channels: band- to-tail recombination (BT), that comprises a free electron and a hole that is localised in the valence band tail; band-to-band recombination (BB), that involves a free electron and a free hole, band-to-impurity (BI) recombination that involves an acceptor state that is deep enough not to overlap with the valence band tail, and donor–acceptor pair (DAP) recombination that involves an acceptor and a donor state that are deep enough not to overlap with the corresponding band tails. All these recombination pathways have been detected in the PL studies of kesterites. In addition to the spatial electrostatic potential fluctuations, detrimental band gap fluctuations due to the structural Cu-Zn disorder and compositional inhomogeneities are present in kesterites, reducing the V_{OC} of the corresponding solar cell devices. One should be aware that the characteristic length of bandgap fluctuations can exceed the typical size of the potential well caused by electrostatic potential fluctuations, allowing localization of electrons in potential minima of the conduction band edge. Typical schematic presentation of a band structure involving both electrostatic and band gap fluctuations is presented in figure 1. Bandgap and electrostatic potential fluctuations contribute to the band tails with a resulting average depth of fluctuations γ that is a combination of both: $\gamma^2 = \gamma_E^2 + \gamma_B^2$, where γ_E and γ_B correspond to the average depth of electrostatic potential and bandgap fluctuations, respectively (see figure 1) [30]. These fluctuations usually determine the asymmetric shape of PL bands, where the shape of the low energy side of the PL spectra is determined by the density of states function. In kesterite samples, γ values in the range $\gamma \approx$ 25–80 meV were found [2, 3, 5, 29, 31–35]. Typical low-temperature measurements for kesterites show a broad peak with increasing width and assymmetry for higher sulfur concentrations as shown in figure 2(a). Figure 2(b) presents a strong dependence of the PL peak emission energy on excitation power commonly observed in kesterites, which is a clear indicator of potential or band gap fluctuations.

There are few publications where very shallow defect levels in CZTSe were measured [36, 37], but a vast majority of PL bands measured in kesterites are further away from the band gap and show an asymmetric and quite wide shape (full width at half maximum >100 meV). In most cases, the dominant recombination is related to the BI transition where free electrons recombine with holes captured by deep acceptor levels. Also band to tail

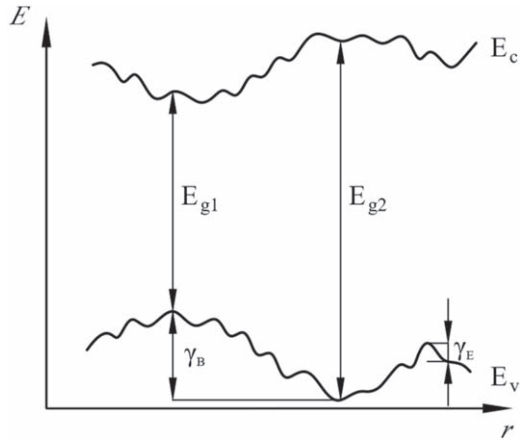

Figure 1. Schematic presentation of the band structure of a semiconductor involving electrostatic and band gap fluctuations. Here, γ_E and γ_B correspond to the average depth of electrostatic potential and bandgap fluctuations, respectively.

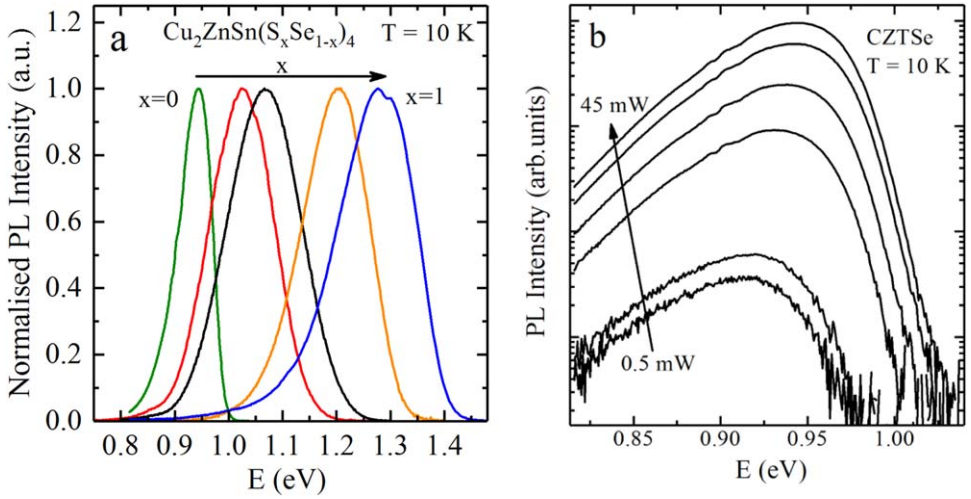

Figure 2. (a) Typical low-temperature PL spectra of $Cu_2ZnSn(S_xSe_{1-x})$ with x varying from 0 to 1 [32], and (b) typical strong excitation power dependence of the PL band in kesterites. (a) Reprinted from [32], Copyright (2011), with permission from Elsevier.

(BT) and band to band (BB) processes have been detected in kesterites [38–42]. In addition, the quasi donor–acceptor pair recombination model is proposed in numerous publications [5, 41, 43, 44]. The word 'quasi' is used to indicate the deviation from the classical DAP model due to interactions between defects. In the case of deep enough acceptor and donor defect levels a different recombination process is possible—deep donor-deep acceptor (DD-DA) pair recombination. DD-DA recombination was detected in many chalcopyrite compounds [45–47] and recently also in CZTS [48].

Theoretical calculations [24, 49] have predicted a low formation energy of several defect clusters in kesterites which may cause a highly localized reduction of the bandgap energy. These defect clusters are likely to be detrimental to device performance, and their presence has been suggested as the dominant recombination pathway for CZTS using low temperature PL [50].

AS, capacitance–voltage, and drive level capacitance profiling (DLCP) have been applied on kesterite semiconductors for the determination of defect transition levels as well as the quantification of deep defects and the doping density ($N_{A,a}$).

Figure 3 shows typical admittance data of a $Cu_2ZnSnSe_{0.4}S_{0.6}$ kesterite solar cell with ~9% efficiency [51]. At low temperatures the capacitance approaches the geometric capacitance due to freeze-out of mobile carriers in the absorber. With increasing temperature two distinct capacitance steps are observed. In the case of a classical semiconductor the first step in the capacitance is interpreted with the dielectric turn-on due to shallow dopants, leveling at the capacitance given by the space-charge region. Capacitance steps occuring at higher temperatures are commonly interpreted as deep defects [5]. In kesterites, this first step is typically observed at significantly higher temperatures than in related semiconductor materials such as $Cu(In,Ga)Se_2$ [52]. This has been explained

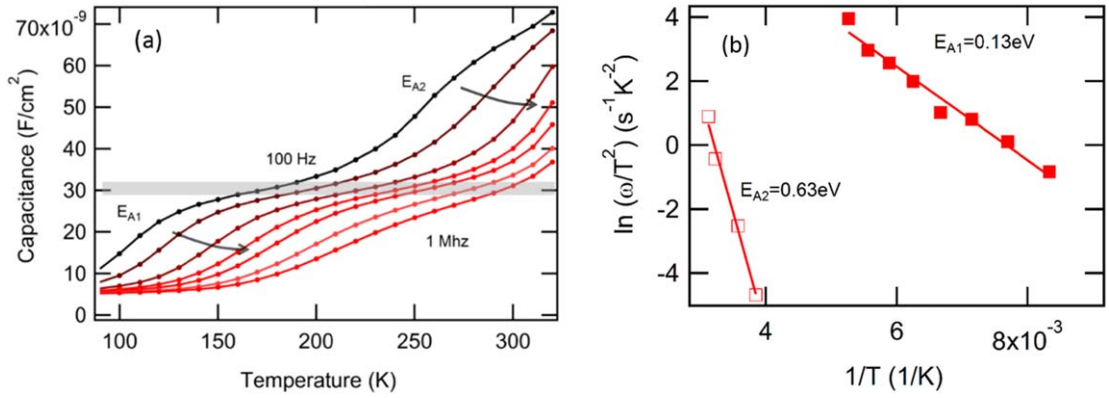

Figure 3. (a) Typical CZTSSe admittance data of a 9% efficient CZTSSe solar cell grown by solution processing [51] (b) Arrhenius plots and activation energies exctracted from capacitance steps in (a).

with a large series resistance in kesterites at low temperatures arising from either too deep acceptors [53] or a barrier at the back contact [54]. A high series resistance alone, even if temperature independent, could lead to a capacitance step due to circuit response if an inadequate equivalent circuit model is used [55], emphasizing the need to use appropriate models to analyze admittance measurements [5, 56, 57]. In the literature no complete agreement on this phenomenon is found, e.g. in [58] it was found that the series resistance and the first capacitance step have similar activation energies varying between 20 and 100 meV depending on the kesterite's annealing conditions, while in [5] it was found that the activation energies were different. In some cases two overlapping steps at low temperature can be observed [58, 59], which however cannot be distinguished in the measurement shown in figure 3(a). Distinguishing multiple steps at low temperature may require deconvolution techniques [58] and can also be strongly influenced by the measurement conditions, i.e. light exposure or carrier injection [59]. The second capacitance step seen in figure 3(a) associated with deep defects has been found to depend on material parameters, such as composition [51] and annealing conditions [21]. Therefore, it is difficult to generalize results found in literature, and all these parameters and conditions have to be taken into account. Energy levels of intrinsic defects in kesterites determined by AS method are summarized in table 1, mostly reporting activation energies >50 meV. This is consistent with the large formation energy of shallow copper vacancies predicted by DFT in kesterite, which suggest the deeper Cu_{Zn} antisite to be the dominant hole donating acceptor level and also a higher carrier-freeze out temperature.

In order to determine the free charge carrier density from admittance measurements or capacitance–voltage profiling, the measurement conditions (temperature and frequency) should be chosen such that the space charge capacitance but not the capacitance due to deep defects is evaluated. Most authors interpret the capacitance above the first step (grey shading in figure 3(a)) as the space charge capacitance [5, 21, 53, 58, 60]. Thus for kesterites, typical measurement conditions to obtain the free carrier density range from (200 K, 1 kHz used in [58]) to (300 K, 100 kHz, used in [51]), which according to figure 3 is expected to yield identical results. Please note that if this first capacitance step would be due to a barrier, the capacitance–voltage profiling with parameters targeting at this plateau still give the correct carrier density, while the space charge region would be slightly overestimated, due to the effect of the barrier [52]. Frequency-dependent capacitance–voltage profiles performed at room-temperature often yield a strong dispersion for kesterites, which indicates that deep defects may be present and respond in the capacitance measurement at lower frequencies [51]. A comparison of the free-carrier densities deduced from capacitance–voltage profiling under different measurement conditions are reported in table S1 (supplementary information available online at stacks.iop.org/JPENERGY/1/044002/mmedia), and (selectively) plotted together with Hall effect results in figure 5 of section 4 further below.

An overview of the defect levels in kesterite materials determined by PL and admittance measurements as well as from the photoconductivity (σ (T)), photocapacitance (TPC) and surface photovoltage (SPV) measurements, is given in table 1. In most publications defect levels deduced from either PL or AS methods are reported, while in [5] a defect level diagram for the solid solution $Cu_2ZnSnS_xSe_{1-x}$ with ($0 < \times < 1$) was constructed from combined PL and admittance measurements. This study proposed the presence of a shallow defect and a deep defect with relatively constant transition levels on an absolute scale, but varying with respect to the valence band edge, because of the upward shift of the valence band maximum with increasing selenium content [5].

According to first-principles calculations the antisite defect Cu_{Zn} has the lowest formation energy and it contributes the most to the p-type conductivity in the stoichiometric kesterites CZTS and CZTSe [24]. The

Table 1. Experimentally determined energy levels of intrinsic defects in kesterites.

Material	S/(S + Se)	Energy level (meV)	Proposed defect	Method	References
CZTSe		$E_V + 27$		PL	[37]
		$E_V + 69$		PL	[61]
			V_{Cu}	PL	[62]
		$E_V + 63$	Zn_{Sn}		
		$E_V + 69$	Cu_{Zn}	PL	[56]
		$E_V + 75$	Cu_{Zn}	AS	
		$E_V + 90$	Cu_{Zn}	PL	[63]
		$E_V + 63$	Zn_{Sn}		
		$E_V + 13$		PL	[36]
		$E_V + 27$			
		$E_C - 7$			
		$E_V + 63$		PL	[64]
		$E_V + 88$			
		$E_V + 40$		PL	[44]
		$E_V + 80$			
		$E_V + 140$	Cu_{Zn}	AS	[65]
		$E_V + 51$	V_{Cu}		
		$E_V + 170$		AS	[66]
		$E_V + 90$		AS	[59]
		$E_V + 157$			
		$E_V + 160$	Cu_{Zn}	AS	[67]
		$E_V + 120$	Cu_{Zn}	PL,AS	[5]
		$E_V + 480$	Cu_{Sn} ; V_{Sn}	DLTS	[68]
		$E_C - 90$	Zn_{Cu}		
		$E_V + 30$	V_{Cu}		
CZTSSe	0.58	$E_V + 120$	Cu_{Zn}	DLTS	[68]
	0.58	$E_V + 320$	Cu_{Sn}		
	0.36	$E_C - 121$	Zn_{Cu}	PL	[29]
	0.28	$E_C - 94$	Zn_{Cu}		
	0.28	$E_V + 301$	Zn_{Sn}	SPV	
	0.28	$E_C - 91$	Zn_{Cu}		
	N/A	$E_V + (130–200)$		AS	[53]
	0.02	$E_V + 39$	V_{Cu}; Cu_{Zn}	PL	[69]
	0.11	$E_V + 63$	$V_{Cu} + Zn_{Cu}$; $Zn_{Sn} + 2Zn_{Cu}$		

Table 1. (Continued.)

Material	S/(S + Se)	Energy level (meV)	Proposed defect	Method	References
	0.35	$E_V + 134$	Cu_{Zn}	AS	[60]
	0.8	$E_V + 163$	Cu_{Zn}		
	0.6	$E_v + 170$	Cu_{Zn}	AS	[5]
	0.6	$E_v + 530$		AS	
	0.6	$E_v + 260$	Cu_{Zn}	PL	
	0.6	$E_C - 130$	Zn_{Cu}		
	0.4	$E_C - 140$	Zn_{Cu}	PL	
	0.4	$E_v + 140$	Cu_{Zn}		
	0.4	$E_v + 500$		AS	
	0.4	$E_v + 130$	Cu_{Zn}		
CZTS		$E_V + 183$	Cu_{Zn}	AS	[60]
		$E_V + 289$	Cu_{Sn}	PL	[70]
		$E_V + 194$		PL	[34]
		$E_V + 62$			
		$E_V + 105$	Cu_{Zn}-Zn_i	PL	[48]
		$E_V + 125$			
		$E_C - 660$	Cu_{Zn}-Sn_{Zn}	PL	[50]
		$E_V + 20$	V_{Cu}	PL	[29]
		$E_V + 40$		PL	[71]
		$E_V + 290$	Cu_{Zn}	AS	[5]
		$E_C - 140$	Zn_{Cu}	AS	
		$E_V + 230$	Cu_{Zn}	PL	
		$E_V + 40$		PL	[72]
		$E_V + 112$	Cu_{Zn}	PL	[73]
		$E_V + 132$	Cu_{Zn}	σ(T)	[74]
		$E_V + 37$		σ(T)	[75]
		$E_V + 45$		AS	[76]
		$E_V + 113$	Cu_{Zn}		
		$E_C - 96$	Zn_{Cu}	AS	[35]
		$E_V + 119$	Cu_{Zn}		
		$E_V + 48$		PL	[77]
		$E_V + 185$		PL	[78]
		$E_V + 140$	Cu_{Zn}	PL	[79]
		$E_V + (276–284)$		PL	[80]
		$E_V + 40$		PL	[71]
		$E_V + 112$		PL	[81]

Table 1. (Continued.)

Material	S/(S + Se)	Energy level (meV)	Proposed defect	Method	References
		$E_V + 114$	Cu_{Zn}	σ(T)	[82]
		$E_V + 300$			
		$E_V + 70$	Cu_{Zn}	σ(T)	[83]
		$E_V + 221$	V_{Sn}		
		$E_V + 1000$		TPC	[84]

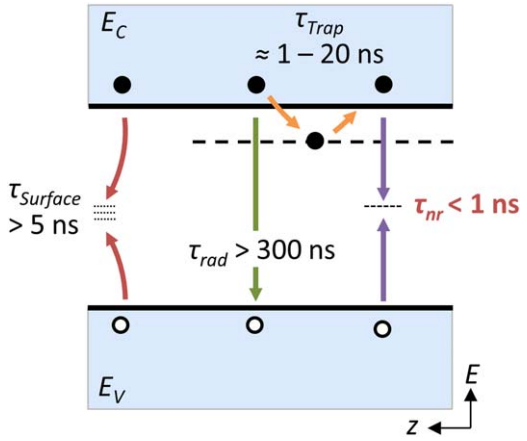

Figure 4. Schematic representation of various recombination mechanisms which contribute to the minority carrier lifetime in kesterites, and their relative impact. τ_{Trap} is the trapping/de-trapping time, $\tau_{surface}$ is the surface recombination lifetime, τ_{rad} is the radiative lifetime in low injection, and τ_{nr} is the non-radiative lifetime.

highest solar cell efficiencies have been achieved at low Cu and high Zn compositions which should decrease the formation of Cu_{Zn} and promote the formation V_{Cu}. The Zn-rich and Cu-poor compositions of CZTS and CZTSe should also help to avoid the formation of detrimental Sn-related deep defects such as Cu_{Sn}, Sn_{Cu} and Sn_{Zn} and associated defect complexes.

A classification system of kesterites based on stoichiometry has been proposed by Lafond *et al* [85] and Gurieva *et al* [86] and includes 12 types corresponding to various defect complexes necessary to achieve a given deviation from stoichiometry (i.e. Cu poor + Zn rich = $[V_{cu} + Zn_{Cu}]$). These concepts and the existence of various stoichiometries modifying defect complexes has been verified via neutron diffraction [86]. It is important to emphasize however, that the defect structure depends not only on the elemental composition but also on the the post-growth cooling process or additional thermal treatments which modify the degree of Cu-Zn disordering in kesterites [9]. It has been shown that with reduced disordering, there is a change in the dominant radiative recombination process, involving deeper defects in the case of a less disordered material [34]. This can be one reason why reduced Cu-Zn disordering does not lead to significant improvement in the device performance. More systematic defect studies that would correlate the intrinsic defects in kesterites to the device performance are needed.

3. The minority carrier lifetime in kesterites

The minority carrier lifetime (τ) is a critical parameter to evaluate when quantifying absorber quality in semiconductors. This parameter is a measure of the net recombination rate of minority carriers in a material. Consequently, τ is directly related to the quasi-fermi level splitting of an absorber and thus the open-circuit voltage (V_{OC}) of corresponding devices—a parameter of particular concern for kesterites. Therefore, investigations into the low V_{OC} in kesterites greatly benefit from (i) accurately determining τ and (ii) determining the rate-limiting recombination mechanism which governs τ.

However, τ cannot be directly measured for a given material, requiring extraction from measurements such as luminescence/photoconductivity/photovoltage decay or quantitative luminescence. For highly defective materials such as kesterites, complex carrier transport and dynamics as well as high recombination rates make accurate extraction of τ quite challenging. For this reason, early reports of τ for kesterite materials suggested reasonably large values between 1 and 20 ns; a comprehensive overview of τ values reported for kesterites can be found in [4]. However, recent work indicates that the real minority carrier lifetime in kesterite materials is in the sub-nanosecond regime [4, 87]. Quantitative PL [4], time-resolved terahertz spectroscopy (TRTS) [87, 88], and device simulation [4, 89] independently suggest τ values of a few hundred picoseconds. Therefore, it seems that a low minority carrier lifetime is a present limit to further advances in kesterite device performance. Presently, defect recombination in the bulk kesterite material via non-radiative defects is suspected as the culprit for the high recombination rate/low lifetime [90], illustrated in figure 4. Therefore, developing formation pathways that reduce defect formation, exploring novel defect passivation schemes, or further advancing cation replacement strategies are transformative opportunities for the next-generation of high-efficiency kesterite photovoltaics.

3.1. Measuring a sub-picosecond lifetime in CZTSSe

To accurately determine the minority carrier lifetime for kesterites, a combination of techniques with consistent results has been used. This strategy is recommended for such non-ideal or early stage materials where numerous electron-defect interaction pathways need to be distinguished. Time-resolved photoluminescence (TRPL) is a common measurement tool used to extract τ, where the characteristic PL decay time is often equated to the minority carrier lifetime. However, for kesterites several factors have demonstrated that the PL decay time is an unreliable estimate for the minority carrier lifetime. First, reported PL decays times between 1 and 20 ns throughout literature do not correlate with the V_{OC} or device efficiency [4]. Second, these reported PL decay times significantly overestimate the expected device performance if interpreted as the lifetime, considering a wide range of simulation parameters [4, 89, 91]. The reported PL decay times would result in V_{OC} values at 65%–75% of the Shockley–Queisser limit ($V_{OC,Max}$) and efficiencies between 14% and 20%. However, corresponding devices have $V_{OC}/V_{OC,Max}$ between 25% and 55% and efficiencies between 1% and 11% [4]. Third, TRPL data measured on devices—at a wide range of bias voltages—generally show negligible bias voltage dependence and/or no change when measured on bare absorbers or devices [4]. However, the presence of such an electric field is expected to have a dramatic effect on the TRPL response time due to charge separation effects. The above arguments are contrary to theoretical expectations from solid state physics. In addition to this, experimental TRPL data for kesterites are generally reported over a small decay range due to the low signal associated with this material (generally around 1 order of magnitude of signal decay), which makes accurate fitting and interpretation difficult [4]. Furthermore, a limited instrument response function in TRPL measurements can obscure fitting of decay times below about 1 ns.

Recent work using high-resolution intensity- and temperature-dependent TRPL has shown that the characteristic PL decay times for kesterites can commonly be attributed to trapping/de-trapping processes in the material rather than the minority carrier lifetime [4, 92]. Trapping is also observed in TRTS measurements [88, 93]. The mechanism and defects involved with this minority carrier trapping is an active area of research [94–97]. Similar results can be expected from photoconductivity decay, photovoltage decay, and related measurements, which probe the decay of excess carriers. In certain cases, trapping/de-trapping may not dominate the decay signal of minority carriers and the recombination lifetime may indeed be measured—as found for CZTS, CZTSe, and CZTSSe single crystals, for example [87, 88, 98]. However, these cases validate the sub-nanosecond lifetime conclusion for kesterites and alternative high time-resolution measurement techniques are needed such as TRTS. The effect of trapping in kesterite thin films can be mitigated in measurements which probe the excess carrier decay through saturation of trap states at elevated excitation intensities or elevated temperatures during measurement [92, 99], however high time-resolution measurement techniques would still be needed to extract τ for kesterites due to fast recombination rates.

As an alternative to carrier decay measurements, the minority carrier lifetime can be extracted from quantitative luminescence analysis. In this approach, τ is related to the internal PL efficiency (η_{PL}) following $\eta_{PL} = \tau B p_0$ where B is the radiative recombination coefficient and p_0 is the free carrier density [4]. For kesterites, relatively low internal PL efficiencies (e.g. $\eta_{PL} < 0.01\%$) are ubiquitous—even for state-of-the-art absorbers. Quantitative analysis indicates that a sub-nanosecond lifetime is responsible for the low PL efficiency found in this material.

3.2. Determining the origin of rate limiting recombination

As τ reflects the net recombination of carriers, this parameter can vary widely [100] depending on the origin of limiting recombination. Therefore, it is important to rule out various loss mechanism to determine where efforts should be applied to improve τ. For kesterites, various limiting loss mechanisms have been proposed. First, interface recombination was suggested early on as a significant contributor to the V_{OC} deficit in kesterites [54, 90, 101]. However, the impact of interface recombination may be misinterpreted in kesterites due to the impact of non-ideal device behavior in data analysis [17, 26]. To achieve a sub-nanosecond recombination lifetime at the absorber surface ($\tau_{Surface}$), a surface recombination velocity (S_F) greater then about 2×10^5 cm s^{-1} is necessary ($\tau_{Surface} \approx$ thickness$/S_F$) [102]; however, a positive conduction band offset extends this range to around 10^7 cm s^{-1} [89, 91]. For CZTSe and CZTSSe, detailed transport modelling/measurements [93, 103] estimate surface recombination velocities below 5×10^4 cm s^{-1}, though values above 10^5 cm s^{-1} are reported for bare absorbers following various surface treatments [104]. Exhaustive failure-mode-and-effect-analysis [90] and device simulations [4, 89, 91, 105] indicate that surface recombination is not the dominant loss mechanism for CZTSe and CZTSSe absorbers at the current level of device performance. However, surface losses (i.e. a reduced V_{OC}) may manifest in the device structure due to unfavorable buffer-absorber band alignment—particularly in pure sulfide CZTS, secondary phases at the buffer-absorber interface, interfacial band gap narrowing, and the absence of charge inversion at hetero-interface [90]. However, these factors are distinct from the intrinsic surface and bulk recombination lifetimes of the kesterite absorber.

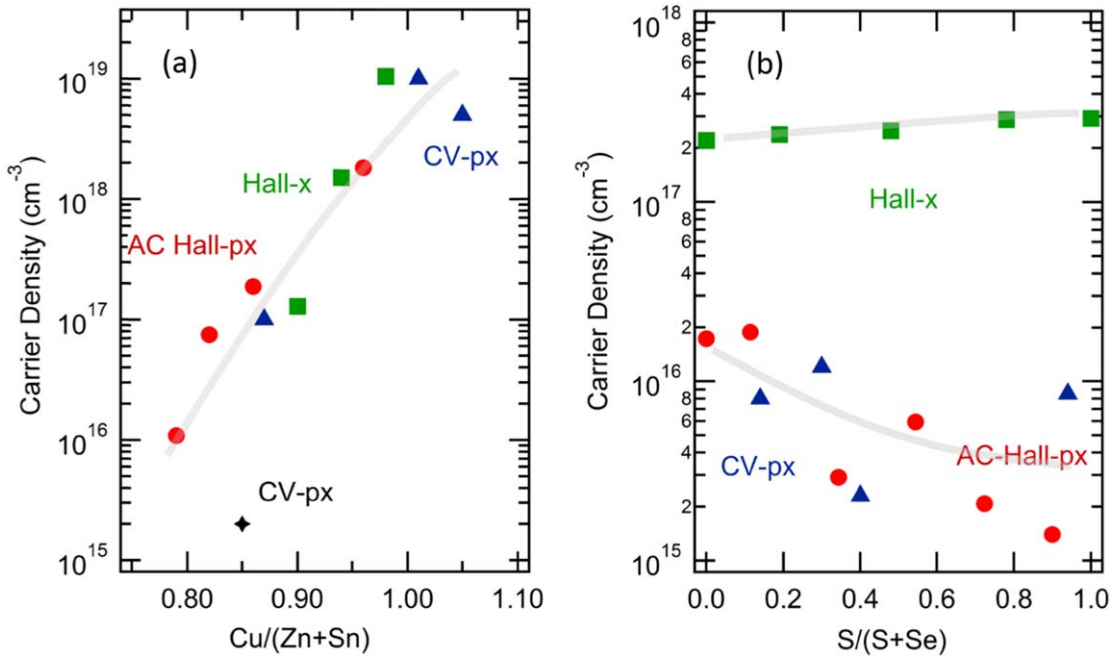

Figure 5. Carrier density from Hall-effect and capacitance–voltage on single crystal films (x) and polycrystalline films (px) as a function of Cu/(Zn + Sn) ratio (a), and as a function of S/(S + Se) ratio (b). Note that not all of the films have the same Zn/Sn and Cu/Sn ratios in (a), and the single crystal samples in (b) have a higher Cu/(Zn + Sn) ratio than the px samples (0.85–0.96).

A general consensus among many kesterite researchers is that limitations in kesterite performance arise from the bulk absorber rather than from its interfaces [90]. Several mechanisms can be responsible for this. First, radiative recombination losses can be disregarded, evident from the low PL yield in this material; a low-injection radiative lifetime (Bp_0) of a few hundred nanoseconds can be expected for CZTSe [4]. This leaves non-radiative losses as a dominant recombination path in the bulk kesterite material. While band tails/potential fluctuations have been significantly studied and observed in kesterites, their role in non-radiative recombination is not straightforward. For shallow defect states to efficiently participate in recombination, their energetic position must lie within the demarcation levels for holes and electrons; shallow defects near the band edges will act as trap centers while deeper defects can participate in recombination. For kesterites, reports vary for the degree of potential fluctuations into the energy gap. Early studies suggest a relatively deep penetration of potential fluctuations into the energy gap which efficiently participate in tunneling-enhanced recombination [17, 26], while recent work suggest shallow potential fluctuations which are not expected to act as efficient recombination centers [4]. However, shallow defects have been suggested to significantly enhance non-radiative recombination through a multistep process [97]. Further work is needed to quantify the role of potential fluctuations/band-tailing on the minority carrier lifetime in kesterites. Next, grain boundary recombination has been reported to contribute to bulk recombination of carriers [90]. Lastly, a more traditional non-radiative recombination mechanism through deep defects in the bulk are expected to play an important role in explaining the significant non-radiative losses measured in kesterites [90, 95]. A relative comparison of the various loss mechanisms discussed here-in is illustrated in the energy band diagram shown in figure 4.

4. Charge carrier transport in kesterites

Carrier transport properties including carrier type, density and mobility are of fundamental importance to all optoelectronic devices. In solar cells, the carrier type (p or n), will determine the device architecture, the majority carrier density affects recombination lifetime and depletion width, while the carrier mobility, specifically for the minority carriers, affects diffusion length which significantly impacts current collection. For CZTSSe, a range of carrier properties have been reported, which may reflect changes in stoichiometry, doping, fabrication method and sample quality, but may also reflect choice of characterization method.

In figure 5(a) carrier densities obtained from both Hall effect and capacitance–voltage profiling are shown as a function of Cu/(Zn + Sn) content. It can be seen that there is a general trend exhibiting an exponential increase in the carrier density as the Cu/(Zn + Sn) ratio increases linearly. Hall measurements clearly indicate p-type doping for CZTSSe of various compositions. The general correlation of carrier concentration and Cu

content is most often ascribed to the dominance of Cu_{Zn} antisite defects, which are predicted to have the lowest formation energy of any defect and provide shallow acceptor states [24]. The defect picture is complicated by extremely high levels of compensated defect complexes, such as [V_{Cu} + Zn_{Cu}], which enable large variations of stoichiometry without equal levels of free carriers. For stoichiometric material, carrier densities of almost 1×10^{19} cm^{-3} are found. For individual compositions very large deviations can be found, e.g. for the record IBM device with a Cu/(Zn + Sn) = 0.85 and S/(S + Se) = 0.25 the carrier density is low 1×10^{15} cm^{-3} [106], while measurements on other samples show up to 1×10^{17} cm^{-3} at the same composition. The data in figure 5 were collected using Hall-effect or capacitance–voltage profiling, which must be performed with distinct sample configurations, the former on absorber layers without back contact, and the latter on a full device structure. Despite the different boundary conditions, the overall agreement is seen to be quite good. Individual samples shown in figure 5(a) may not only vary in copper-content but may also differ somewhat in the Zn/Sn content and sulfur content, and of course sample processing, sodium content, and possibly more. An important point to consider is also that compositional analysis is performed using a variety of different methods in different labs, including inductively coupled plasma mass spectrometry, x-ray fluorescence and energy dispersive x-ray spectroscopy. In addition to calibration challenges and/or different depth bias, these composition measurements usually do not distinguish between the kesterite main phase and the sample composition that includes secondary phases. Thus, similar sample compositions with different secondary phase content may exhibit significantly different compositions of the kesterite phase, as discussed in detail by Just *et al* [107, 108].

Figure 5(b) shows the carrier densities for various samples as a function of S/(S + Se) content for Cu-poor samples. It can be seen that the carrier density varies generally much less than for changing copper content, but tends to decrease for the polycrystalline films with increasing sulfur content, while it slightly increases with sulfur content for the single crystals. The fact that the single crystal values are about an order of magnitude higher and behave different from the polycrystalline films is likely related to the fact the the crystals are near-stoichiometric, compared to the Cu-poor composition of the polycrystalline films. Again, in this figure good overall agreement can be found between carrier densities derived from Hall measurements and those from (room-temperature) capacitance measurements, which indicates that both methods may be reliably applied to estimate charge carrier densities. Best devices typically contain about 20%–30% sulfur and are Cu-poor for which figure 5 would predict a carrier density below 10^{16} cm^{-3}, which indeed has been reported for IBM's champion device [106].

Sodium has been found to be instrumental in increasing the carrier density in Cu-poor Cu(In, Ga)Se_2, which is achieved either from diffusion of the soda-lime glass or by NaF precursor layers, or post-deposition treatments with NaF [109, 110]. The effect of sodium incorporation in CZTSSe has been investigated in several studies on thin films as well as single crystals [111]. In these studies, the increase in the sodium content is generally found to increase the carrier density as measured by Hall effect, although in one recent study a systematic decrease of the carrier density with increasing sodium content was reported [112]. In this study, a NaF layer was deposited and diffused into the absorber after the CZTSe was grown.

For solar cell applications the charge carrier transport to and from electrodes and within the active semiconductor layer plays an important role. The transport of carriers can take place either by drift in electric fields or by diffusion. For both phenomena the carrier mobilities play a decisive role and depending on the type of material and measurement method used can span a very wide range of values from below 1 cm^2 V^{-1} s^{-1} for amorphous semiconductors to several thousand cm^2 V^{-1} s^{-1} for epitaxial GaAs. Charge carrier mobilities depend on fundamental material properties such as the band structure, in particular the effective masses of the conduction band minimum and valence band maximum, carrier-impurity and carrier-phonon scattering as well as grain boundary scattering, and possible trapping in localized states. Different experimental measurement techniques can be applied to derive the carrier mobility, such as Hall effect [74, 113–116], Thz spectroscopy (TRTS) [93, 117–120], or voltage-dependent IQE measurements [17, 121]. In contrast to the good agreement of different measurement techniques for the estimation of carrier densities, for carrier mobilities the repercussions of the different required sample geometries often lead to very different results. It is important to stress that the Hall effect is dominated by majority carrier transport while TRTS measurements capture the sum mobility for minority and majority carriers. In a solar cells, on the other hand, carrier transport is generally dominated by minority carriers [93]. In addition, both Hall effect and TRTS are commonly performed on samples without conducting back contact, however for TRTS it has recently been shown that measurements in reflection geometry on back contact substrates also lead to very good results [119].

Figure 6 shows the mobilities as derived from Hall effect and Thz absorption on single crystals (x) and polycrystalline films (px).

Looking at figure 6(a), which displays mobilities as a function of S/(S + Se) content, it is obvious that the carrier mobilities have a huge range of values from about 0.5 cm^2 V^{-1} s^{-1} to more than 100 cm^2 V^{-1} s^{-1}. A more detailed inspection reveals that the Hall mobilities for the single crystals agree with the TRTS measurements on single crystals as well as TRTS on thin films, while the Hall measurements on polycrystalline

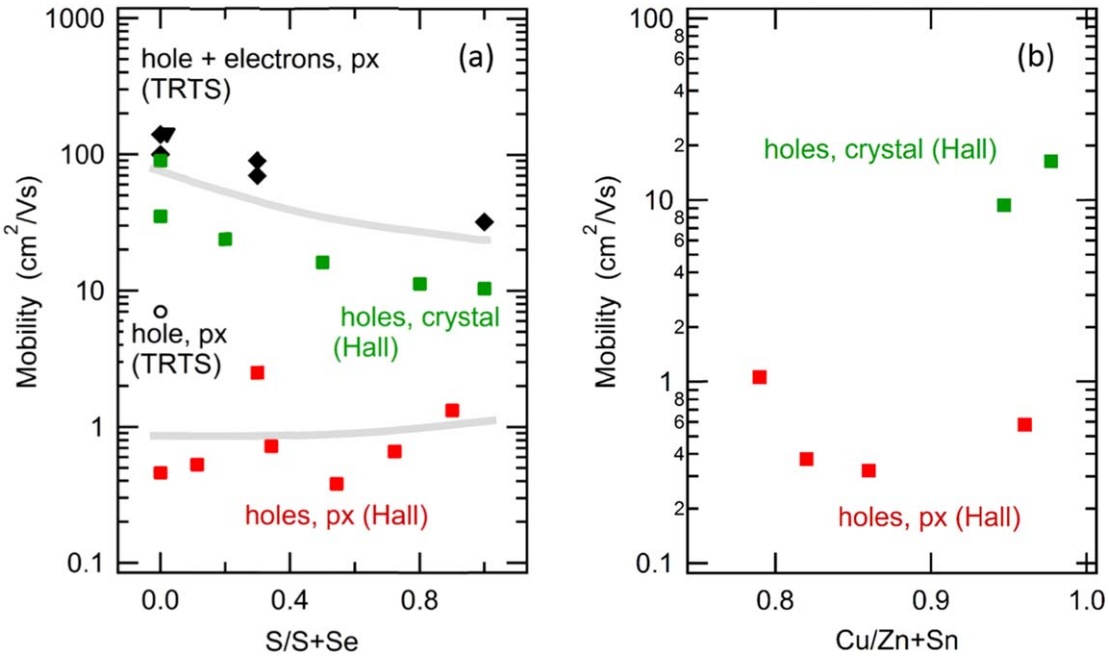

Figure 6. Mobilities from Hall and Thz Absorption (TRTS) for single crystal (x) and polycrystalline films (px), as a function of S/(S + Se) (a) and Cu/(Zn + Sn) (b).

films yield much lower values typically below 1 $cm^2\ V^{-1}\ s^{-1}$. This indicates that grain boundary scattering plays a decisive role in the long-range carrier transport, as TRTS measurements in fact probe intragrain transport on a scale of about 30 nm, and single crystals per definition do not have grain boundaries. Overall, the TRTS and Hall measurements on single crystals show a decrease of carrier mobility from pure CZTSe with 140 $cm^2\ V^{-1}\ s^{-1}$ to about 10–40 $cm^2\ V^{-1}\ s^{-1}$ for the pure sulfide. The larger values of the TRTS measurements compared to Hall in this case can be explained with the fact that Hall measurements probe the majority (hole) mobility and TRTS probes the hole + electron mobility. The true minority carrier mobility can be estimated by substracting the x-Hall values from the TRTS-px values, which leads to values slightly smaller than the TRTS values displayed in figure 6. Majority and minority carrier mobilities have recently been extracted using a new photo-Hall technique [117], as well as from intensity dependent and excitation wavelength dependent TRTS analysis [93]. In the TRTS analysis it was found that for a pure CZTSe polycrystalline layer the electron mobility can be estimated at 140 $cm^2\ V^{-1}\ s^{-1}$ while the hole mobility was significantly lower at about 10 $cm^2\ V^{-1}\ s^{-1}$.

As already mentioned grain boundary scattering is expected to affect the carrier mobility, in particular in the case of non-vanishing grain boundary potentials. Comparing the Hall effect hole mobilities measured on single crystals and on polycrystalline thin films in figure 6, we see that grain boundary potentials in kesterites must be larger than kT in order to explain the difference between these measurements. Whether intra-grain transport or transport across grain boundaries is limiting in solar cells strongly depends on the device geometry and sample microstructure i.e. if the grain sizes are large enough (~500 nm) then carrier absorbed in a single grain most likely do not have to cross a grain boundary in order to reach the pn-junction. On the other hand, for very small-grained material, grain boundaries may well limit transport processes in the devices.

The effect of Cu-Zn ordering on solar cells has been subject of numerous investigations. Recently, the effect of the amount of disorder present in CZTSe films on the carrier mobility was investigated by TRTS measurements [120]. Here it was found that samples with different degrees of Cu-Zn cation ordering showed no change in the charge carrier mobility, which indicates that the cation-ordering is not the limiting phenomenon for the charge carrier mobility in kesterite $Cu_2ZnSn(S_xSe_{1-x})_4$.

5. Summary and outlook

The optical and electrical properties of kesterite $Cu_2ZnSn(S_xSe_{1-x})_4$ absorber materials for solar cells have been extensively studied over the past decade and with the evolution of the performance of the solar cells the knowledge about the fundamental physical properties of the kesterites has been improved. From the basic properties, the band structure of kesterite materials has been extensively studied by various experimental methods. It is clear by now that there is direct relationship between the Cu-Zn disorder and the band gap energy

of kesterites, an increase in the band gap of about 110 and 200 meV can be obtained by changing the order parameter from 0 to 0.7 in CZTSe and CZTS, respectively. On the other hand, several studies have found no clear correlation between the Cu-Zn disorder and charge carrier mobility as well as the V_{OC} deficit of the solar cells.

The studies of intrinsic defects by different experimental methods have shown the presence of rather deep defect levels within the band gap of kesterites. In addition to the rather deep defect levels, the bulk recombination was found to also involve the extended band tail states. The average depth of the band edge fluctuations was found in the range 25–80 meV. The current understanding is that non-radiative recombination in the bulk kesterite is behind the overall low luminescence yield of these materials leading to a high recombination rate and short carrier lifetime in kesterites.

Recent publications which report that the true minority carrier lifetime in kesterites is in the range of a few hundred picoseconds is of particular concern in improvement of the kesterite solar cell device performance. Therefore, developing formation pathways which reduce defect formation, exploring novel defect passivation schemes, or further advancing cation replacement strategies are transformative opportunities for the next-generation of high-efficiency kesterites photovoltaics. Further work is also needed to quantify the role of band edge fluctuations and grain boundaries on the minority carrier lifetime in kesterites.

An overview of the charge carrier transport indicates good agreement between the values of the carrier densities obtained with different characterization techniques despite the fact that they require distinct sample configurations for the measurements. Different conclusions can be made about the determination of the carrier mobility values by using different methods. Comparison of the Hall and Thz spectroscopy results from single crystal and polycrystalline thin film samples indicates that grain boundary scattering plays a decisive role in the long range carrier transport in kesterites, which however is not expected to limit (perpendicular) intragrain transport in absorber layers used in typical thin film solar cells.

Acknowledgments

This work was supported by institutional research funding IUT19–28 of the Estonian Ministry of Education and Research and by the European Union through the European Regional Development Fund, Project TK141, by the European Union through project Starcell (no 720907).

ORCID iDs

Maarja Grossberg https://orcid.org/0000-0003-3357-189X
Douglas M Bishop https://orcid.org/0000-0002-2924-6376

References

[1] Ito K 2014 *Copper Zinc Tin Sulfide-Based Thin-Film Solar Cells* ed K Ito (New York: Wiley) (https://doi.org/10.1002/9781118437865)
[2] Rey G, Larramona G, Bourdais S, Choné C, Delatouche B, Jacob A, Dennler G and Siebentritt S 2018 On the origin of band-tails in kesterite *Sol. Energy Mater. Sol. Cells* **179** 142–51
[3] Gokmen T, Gunawan O, Todorov T K and Mitzi D B 2013 Band tailing and efficiency limitation in kesterite solar cells *Appl. Phys. Lett.* **103** 103506
[4] Hages C J, Redinger A, Levcenko S, Hempel H, Koeper M J, Agrawal R, Greiner D, Kaufmann C A and Unold T 2017 Identifying the real minority carrier lifetime in nonideal semiconductors: a case study of kesterite *Mater. Adv. Energy Mater.* **7** 1700167
[5] Levcenko S, Just J, Redinger A, Larramona G, Bourdais S, Dennler G, Jacob A and Unold T 2016 Deep defects in $Cu_2ZnSn(S, Se)_4$ solar cells with varying Se content *Phys. Rev. Appl.* **5** 024004
[6] Schorr S 2011 The crystal structure of kesterite type compounds: a neutron and x-ray diffraction study *Sol. Energy Mater. Sol. Cells* **95** 1482–8
[7] Choubrac L, Lafond A, Paris M, Guillot-Deudon C and Jobic S 2015 The stability domain of the selenide kesterite photovoltaic materials and NMR investigation of the Cu/Zn disorder in Cu_2 $ZnSnSe_4$ (CZTSe) *Phys. Chem. Chem. Phys.* **17** 15088–92
[8] Chen S, Gong X G, Walsh A and Wei S-H 2009 Electronic structure and stability of quaternary chalcogenide semiconductors derived from cation cross-substitution of II-VI and I-III-VI_2 compounds *Phys. Rev.* B **79** 165211
[9] Scragg J J S, Choubrac L, Lafond A, Ericson T and Platzer-Björkman C 2014 A low-temperature order-disorder transition in Cu_2ZnSnS_4 thin films *Appl. Phys. Lett.* **104** 041911
[10] Rey G, Redinger A, Sendler J, Weiss T P, Thevenin M, Guennou M, El Adib B and Siebentritt S 2014 The band gap of $Cu_2ZnSnSe_4$: effect of order-disorder *Appl. Phys. Lett.* **105** 112106
[11] Vineyard G H 1956 Theory of order-disorder kinetics *Phys. Rev.* **102** 981–92
[12] Többens D M, Gurieva G, Levcenko S, Unold T and Schorr S 2016 Temperature dependency of Cu/Zn ordering in CZTSe kesterites determined by anomalous diffraction *Phys. Status Solidi* **253** 1890–7
[13] Valentini M, Malerba C, Menchini F, Tedeschi D, Polimeni A, Capizzi M and Mittiga A 2016 Effect of the order-disorder transition on the optical properties of Cu_2ZnSnS_4 *Appl. Phys. Lett.* **108** 211909
[14] Hirate Y, Tampo H, Minoura S, Kadowaki H, Nakane A, Kim K M, Shibata H, Niki S and Fujiwara H 2015 Dielectric functions of $Cu_2ZnSnSe_4$ and Cu_2SnSe_3 semiconductors *J. Appl. Phys.* **117** 015702

[15] Li S-Y, Hägglund C, Ren Y, Scragg J J S, Larsen J K, Frisk C, Rudisch K, Englund S and Platzer-Björkman C 2016 Optical properties of reactively sputtered Cu_2ZnSnS_4 solar absorbers determined by spectroscopic ellipsometry and spectrophotometry *Sol. Energy Mater. Sol. Cells* **149** 170–8

[16] Li S, Zamulko S, Persson C, Ross N, Larsen J K and Platzer-Björkman C 2017 Optical properties of $Cu_2ZnSn(S_xSe_{1-x})_4$ solar absorbers: spectroscopic ellipsometry and *ab initio* calculations *Appl. Phys. Lett.* **110** 021905

[17] Hages C J, Carter N J and Agrawal R 2016 Generalized quantum efficiency analysis for non-ideal solar cells: case of $Cu_2ZnSnSe_4$ *J. Appl. Phys.* **119** 014505

[18] Choi S 2018 $Cu_2ZnSn(S, Se)_4$ and related materials *Springer Series in Optical Sciences* (Berlin: Springer) pp 333–55

[19] Zamulko S, Berland K and Persson C 2018 Optical properties of $Cu_2ZnSn(S_xSe_{1-x})_4$ by first-principles calculations *Phys. Status Solidi* **215** 1700945

[20] Nishiwaki M, Nagaya K, Kato M, Fujimoto S, Tampo H, Miyadera T, Chikamatsu M, Shibata H and Fujiwara H 2018 Tail state formation in solar cell materials: first principles analyses of zincblende, chalcopyrite, kesterite, and hybrid perovskite crystals *Phys. Rev. Mater.* **2** 085404

[21] Rey G, Weiss T P, Sendler J, Finger A, Spindler C, Werner F, Melchiorre M, Hála M, Guennou M and Siebentritt S 2016 Ordering kesterite improves solar cells: a low temperature post-deposition annealing study *Sol. Energy Mater. Sol. Cells* **151** 131–8

[22] Lang M, Renz T, Mathes N, Neuwirth M, Schnabel T, Kalt H and Hetterich M 2016 Influence of the Cu content in $Cu_2ZnSn(S, Se)_4$ solar cell absorbers on order-disorder related band gap changes *Appl. Phys. Lett.* **109** 142103

[23] Bourdais S *et al* 2016 Is the Cu/Zn disorder the main culprit for the voltage deficit in kesterite solar cells? *Adv. Energy Mater.* **6** 1502276

[24] Chen S, Walsh A, Gong X-G and Wei S-H 2013 Classification of lattice defects in the kesterite Cu_2ZnSnS_4 and $Cu_2ZnSnSe_4$ earth-abundant solar cell absorbers *Adv. Mater.* **25** 1522–39

[25] Gunawan O, Gokmen T and Mitzi D B 2014 Suns-V_{OC} characteristics of high performance kesterite solar cells *J. Appl. Phys.* **116** 084504

[26] Hages C J, Carter N J, Agrawal R and Unold T 2014 Generalized current–voltage analysis and efficiency limitations in non-ideal solar cells: case of $Cu_2ZnSn(S_xSe_{1-x})_4$ and $Cu_2Zn(Sn_yGe_{1-y})(S_xSe_{1-x})_4$ *J. Appl. Phys.* **115** 234504

[27] Levanyuk A P and Osipov V V 1981 Edge luminescence of direct-gap semiconductors *Sov. Phys. Usp.* **24** 187–215

[28] Krustok J, Collan H, Yakushev M and Hjelt K 1999 The role of spatial potential fluctuations in the shape of the PL bands of multinary semiconductor compounds *Phys. Scr.* **T79** 179–82

[29] Lin X, Ennaoui A, Levcenko S, Dittrich T, Kavalakkatt J, Kretzschmar S, Unold T and Lux-Steiner M C 2015 Defect study of $Cu_2ZnSn(S_xSe_{1-x})_4$ thin film absorbers using photoluminescence and modulated surface photovoltage spectroscopy *Appl. Phys. Lett.* **106** 013903

[30] Werner J H, Mattheis J and Rau U 2005 Efficiency limitations of polycrystalline thin film solar cells: case of Cu(In, Ga)Se_2 *Thin Solid Films* **480–481** 399–409

[31] Krustok J, Josepson R, Raadik T and Danilson M 2010 Potential fluctuations in $Cu_2ZnSnSe_4$ solar cells studied by temperature dependence of quantum efficiency curves *Physica* B **405** 3186–9

[32] Grossberg M, Krustok J, Raudoja J, Timmo K, Altosaar M and Raadik T 2011 Photoluminescence and Raman study of $Cu_2ZnSn(Se_xS_{1-x})_4$ monograins for photovoltaic applications *Thin Solid Films* **519** 7403–6

[33] Yakushev M V, Sulimov M A, Márquez-Prieto J, Forbes I, Edwards P R, Zhivulko V D, Borodavchenko O M, Mudryi A V, Krustok J and Martin R W 2019 A luminescence study of Cu_2 $ZnSnSe_4$/Mo/glass films and solar cells with near stoichiometric copper content *J. Phys. D: Appl. Phys.* **52** 055502

[34] Grossberg M, Krustok J, Raadik T, Kauk-Kuusik M and Raudoja J 2014 Photoluminescence study of disordering in the cation sublattice of Cu_2ZnSnS_4 *Curr. Appl. Phys.* **14** 1424–7

[35] Yin L, Cheng G, Feng Y, Li Z, Yang C and Xiao X 2015 Limitation factors for the performance of kesterite Cu_2ZnSnS_4 thin film solar cells studied by defect characterization *RSC Adv.* **5** 40369–74

[36] Yakushev M V, Forbes I, Mudryi A V, Grossberg M, Krustok J, Beattie N S, Moynihan M, Rockett A and Martin R W 2015 Optical spectroscopy studies of $Cu_2ZnSnSe_4$ thin films *Thin Solid Films* **582** 154–7

[37] Luckert F *et al* 2011 Optical properties of high quality $Cu_2ZnSnSe_4$ thin films *Appl. Phys. Lett.* **99** 062104

[38] Grossberg M, Salu P, Raudoja J and Krustok J 2013 Microphotoluminescence study of Cu_2ZnSnS_4 polycrystals *J. Photonics Energy* **3** 030599

[39] Romero M J, Du H, Teeter G, Yan Y and Al-Jassim M M 2011 Comparative study of the luminescence and intrinsic point defects in the kesterite Cu_2ZnSnS_4 and chalcopyrite Cu(In, Ga)Se_2 thin films used in photovoltaic applications *Phys. Rev.* B **84** 165324

[40] Tanaka K, Shinji T and Uchiki H 2014 Photoluminescence from Cu_2ZnSnS_4 thin films with different compositions fabricated by a sputtering-sulfurization method *Sol. Energy Mater. Sol. Cells* **126** 143–8

[41] Tai K F, Gershon T, Gunawan O and Huan C H A 2015 Examination of electronic structure differences between CIGSSe and CZTSSe by photoluminescence study *J. Appl. Phys.* **117** 235701

[42] Yakushev M V, Márquez-Prieto J, Forbes I, Edwards P R, Zhivulko V D, Mudryi A V, Krustok J and Martin R W 2015 Radiative recombination in $Cu_2ZnSnSe_4$ thin films with Cu deficiency and Zn excess *J. Phys. D: Appl. Phys.* **48** 475109

[43] Gershon T, Shin B, Bojarczuk N, Gokmen T, Lu S and Guha S 2013 Photoluminescence characterization of a high-efficiency Cu_2ZnSnS_4 device *J. Appl. Phys.* **114** 154905

[44] Oueslati S, Brammertz G, Buffière M, Köble C, Oualid T, Meuris M and Poortmans J 2015 Photoluminescence study and observation of unusual optical transitions in $Cu_2ZnSnSe_4$/CdS/ZnO solar cells *Sol. Energy Mater. Sol. Cells* **134** 340–5

[45] Krustok J, Raudoja J, Krunks M, Mändar H and Collan H 2000 Nature of the native deep localized defect recombination centers in the chalcopyrite and orthorhombic $AgInS_2$ *J. Appl. Phys.* **88** 205–9

[46] Krustok J, Raudoja J, Schön J H, Yakushev M and Collan H 2000 Role of deep donor-deep acceptor complexes in CIS-related compounds *Thin Solid Films* **361** 406–10

[47] Krustok J, Schön J H, Collan H, Yakushev M, Mädasson J and Bucher E 2001 Erratum: origin of the deep center photoluminescence in $CuGaSe_2$ and $CuInS_2$ crystals [J. Appl. Phys. 86, 364 (1999)] *J. Appl. Phys.* **89** 8357–8

[48] Krustok J, Raadik T, Grossberg M, Kauk-Kuusik M, Trifiletti V and Binetti S 2018 Photoluminescence study of deep donor- deep acceptor pairs in Cu_2ZnSnS_4 *Mater. Sci. Semicond. Process.* **80** 52–5

[49] Huang D and Persson C 2013 Band gap change induced by defect complexes in Cu_2ZnSnS_4 *Thin Solid Films* **535** 265–9

[50] Grossberg M, Raadik T, Raudoja J and Krustok J 2014 Photoluminescence study of defect clusters in Cu_2ZnSnS_4 polycrystals *Curr. Appl. Phys.* **14** 447–50

[51] Larramona G, Levcenko S, Bourdais S, Jacob A, Choné C, Delatouche B, Moisan C, Just J, Unold T and Dennler G 2015 Fine-tuning the Sn content in CZTSSe thin films to achieve 10.8% solar cell efficiency from spray-deposited water-ethanol-based colloidal inks *Adv. Energy Mater.* **5** 1501404

[52] Eisenbarth T, Unold T, Caballero R, Kaufmann C A and Schock H-W 2010 Interpretation of admittance, capacitance–voltage, and current-voltage signatures in Cu(In, Ga)Se_2 thin film solar cells *J. Appl. Phys.* **107** 034509

[53] Gunawan O, Gokmen T, Warren C W, Cohen J D, Todorov T K, Barkhouse D A R, Bag S, Tang J, Shin B and Mitzi D B 2012 Electronic properties of the $Cu_2ZnSn(Se, S)_4$ absorber layer in solar cells as revealed by admittance spectroscopy and related methods *Appl. Phys. Lett.* **100** 253905

[54] Gunawan O, Todorov T K and Mitzi D B 2010 Loss mechanisms in hydrazine-processed $Cu_2ZnSn(Se, S)_4$ solar cells *Appl. Phys. Lett.* **97** 233506

[55] Scofield J H 1995 Effects of series resistance and inductance on solar cell admittance measurements *Sol. Energy Mater. Sol. Cells* **37** 217–33

[56] Kask E, Grossberg M, Josepson R, Salu P, Timmo K and Krustok J 2013 Defect studies in $Cu_2ZnSnSe_4$ and $Cu_2ZnSn(Se_{0.75}S_{0.25})_4$ by admittance and photoluminescence spectroscopy *Mater. Sci. Semicond. Process.* **16** 992–6

[57] Bodeux R, Rousset J, Tsin F, Mollica F, Leite E and Delbos S 2018 Determination of the electronic properties of $Cu_2ZnSnSe_4$-based solar cells by impedance spectroscopy and current–voltage characteristics analysis *Appl. Phys.* A **124** 22

[58] Weiss T P, Redinger A, Rey G, Schwarz T, Spies M, Cojocura-Mirédin O, Choi P-P and Siebentritt S 2016 Impact of annealing on electrical properties of $Cu_2ZnSnSe_4$ absorber layers *J. Appl. Phys.* **120** 045703

[59] Koeper M J, Hages C J, Li J V, Levi D and Agrawal R 2017 Metastable defect response in CZTSSe from admittance spectroscopy *Appl. Phys. Lett.* **111** 142105

[60] Duan H-S, Yang W, Bob B, Hsu C-J, Lei B and Yang Y 2013 The role of sulfur in solution-processed $Cu_2ZnSn(S, Se)_4$ and its effect on defect properties *Adv. Funct. Mater.* **23** 1466–71

[61] Grossberg M, Krustok J, Timmo K and Altosaar M 2009 Radiative recombination in $Cu_2ZnSnSe_4$ monograins studied by photoluminescence spectroscopy *Thin Solid Films* **517** 2489–92

[62] Márquez-Prieto J *et al* 2016 Impact of the selenisation temperature on the structural and optical properties of CZTSe absorbers *Sol. Energy Mater. Sol. Cells* **152** 42–50

[63] Yakushev M V, Sulimov M A, Márquez-Prieto J, Forbes I, Krustok J, Edwards P R, Zhivulko V D, Borodavchenko O M, Mudryi A V and Martin R W 2017 Influence of the copper content on the optical properties of CZTSe thin films *Sol. Energy Mater. Sol. Cells* **168** 69–77

[64] Yakushev M V *et al* 2018 Effects of Ar^+ etching of $Cu_2ZnSnSe_4$ thin films: an x-ray photoelectron spectroscopy and photoluminescence study *J. Vac. Sci. Technol.* B **36** 061208

[65] Li J, Kim S, Nam D, Liu X, Kim J, Cheong H, Liu W, Li H, Sun Y and Zhang Y 2017 Tailoring the defects and carrier density for beyond 10% efficient CZTSe thin film solar cells *Sol. Energy Mater. Sol. Cells* **159** 447–55

[66] Brammertz G *et al* 2015 Investigation of properties limiting efficiency in $Cu_2ZnSnSe_4$-based solar cells *IEEE J. Photovolt.* **5** 649–55

[67] Kim Y and Choi I-H 2016 Defect characterization in co-evaporated $Cu_2ZnSnSe_4$ thin film solar cell *Curr. Appl. Phys.* **16** 944–8

[68] Das S, Chaudhuri S K, Bhattacharya R N and Mandal K C 2014 Defect levels in $Cu_2ZnSn(S_xSe_{1-x})_4$ solar cells probed by current-mode deep level transient spectroscopy *Appl. Phys. Lett.* **104** 192106

[69] Campbell S, Qu Y, Bowen L, Chapon P, Barrioz V, Beattie N S and Zoppi G 2018 Influence of OLA and FA ligands on the optical and electronic properties of $Cu_2ZnSn(S, Se)_4$ thin films and solar cells prepared from nanoparticle inks *Sol. Energy* **175** 101–9

[70] Grossberg M, Krustok J, Raudoja J and Raadik T 2012 The role of structural properties on deep defect states in Cu_2ZnSnS_4 studied by photoluminescence spectroscopy *Appl. Phys. Lett.* **101** 102102

[71] Yamazaki M, Nakagawa M, Jimbo K, Shimamune Y and Katagiri H 2017 Photoluminescence study of Cu_2ZnSnS_4 thin film solar cells *Phys. Status Solidi* C **14** 1600202

[72] Leitão J P, Santos N M, Fernandes P A, Salomé P M P, da Cunha A F, González J C, Ribeiro G M and Matinaga F M 2011 Photoluminescence and electrical study of fluctuating potentials in Cu_2ZnSnS_4 -based thin films *Phys. Rev.* B **84** 024120

[73] Li X, Cao H, Dong Y, Yue F, Chen Y, Xiang P, Sun L, Yang P and Chu J 2017 Investigation of Cu_2ZnSnS_4 thin films with controllable Cu composition and its influence on photovoltaic properties for solar cells *J. Alloys Compd.* **694** 833–40

[74] Nagaoka A, Miyake H, Taniyama T, Kakimoto K and Yoshino K 2013 Correlation between intrinsic defects and electrical properties in the high-quality Cu_2ZnSnS_4 single crystal *Appl. Phys. Lett.* **103** 112107

[75] Muhunthan N, Singh P O, Singh N V, Sood N K and Kumari R 2015 Electric field-effect-assisted persistent photoconductivity in CZTS *Adv. Mater. Lett.* **6** 290–3

[76] Fernandes P A, Sartori A F, Salomé P M P, Malaquias J, da Cunha A F, Graça M P F and González J C 2012 Admittance spectroscopy of Cu_2ZnSnS_4 based thin film solar cells *Appl. Phys. Lett.* **100** 233504

[77] Tanaka K, Miyamoto Y, Uchiki H, Nakazawa K and Araki H 2006 Donor-acceptor pair recombination luminescence from Cu_2ZnSnS_4 bulk single crystals *Phys. Status Solidi* **203** 2891–6

[78] Mendis B G, Shannon M D, Goodman M C, Major J D, Claridge R, Halliday D P and Durose K 2014 Direct observation of Cu, Zn cation disorder in Cu_2ZnSnS_4 solar cell absorber material using aberration corrected scanning transmission electron microscopy *Prog. Photovolt. Res. Appl.* **22** 24–34

[79] Levcenko S, Tezlevan V E, Arushanov E, Schorr S and Unold T 2012 Free-to-bound recombination in near stoichiometric Cu_2ZnSnS_4 single crystals *Phys. Rev.* B **86** 045206

[80] Teixeira J P, Sousa R A, Sousa M G, da Cunha A F, Fernandes P A, Salomé P M P and Leitão J P 2014 Radiative transitions in highly doped and compensated chalcopyrites and kesterites: the case of Cu_2ZnSnS_4 *Phys. Rev.* B **90** 235202

[81] Phuong L Q, Okano M, Yamada Y, Nagaoka A, Yoshino K and Kanemitsu Y 2014 Temperature-dependent photocarrier recombination dynamics in Cu_2ZnSnS_4 single crystals *Appl. Phys. Lett.* **104** 081907

[82] Rakhshani A E 2016 Solution-grown near-stoichiometry Cu_2ZnSnS_4 films: optical transitions and defect levels *J. Alloys Compd.* **675** 387–92

[83] Rakhshani A E and Thomas S 2015 Cu_2ZnSnS_4 films grown on flexible substrates by dip coating using a methanol-based solution: electronic properties and devices *J. Electron. Mater.* **44** 4760–8

[84] Islam M M, Halim M A, Sakurai T, Sakai N, Kato T, Sugimoto H, Tampo H, Shibata H, Niki S and Akimoto K 2015 Determination of deep-level defects in $Cu_2ZnSn(S,Se)_4$ thin-films using photocapacitance method *Appl. Phys. Lett.* **106** 243905

[85] Lafond A, Choubrac L, Guillot-Deudon C, Deniard P and Jobic S 2012 Crystal structures of photovoltaic chalcogenides, an intricate puzzle to solve: the cases of CIGSe and CZTS *Mater. Z. Anorg. Allg. Chem.* **638** 2571–7

[86] Gurieva G, Valle Rios L E, Franz A, Whitfield P and Schorr S 2018 Intrinsic point defects in off-stoichiometric $Cu_2ZnSnSe_4$: a neutron diffraction study *J. Appl. Phys.* **123** 161519

[87] Li S, Lloyd M A, Hempel H, Hages C J, Márquez J A, Unold T, Eichberger R, McCandless B E and Baxter J B 2019 Relating carrier dynamics and photovoltaic device performance of single-crystalline $Cu_2ZnSnSe_4$ *Phys. Rev. Appl.* **11** 034005

[88] Phuong L Q, Okano M, Yamada Y, Yamashita G, Morimoto T, Nagai M, Ashida M, Nagaoka A, Yoshino K and Kanemitsu Y 2014 Ultrafast free-carrier dynamics in Cu_2ZnSnS_4 single crystals studied using femtosecond time-resolved optical spectroscopy *Appl. Phys. Lett.* **105** 231902

[89] Kanevce A, Repins I and Wei S-H 2015 Impact of bulk properties and local secondary phases on the $Cu_2(Zn, Sn)Se_4$ solar cells open-circuit voltage *Sol. Energy Mater. Sol. Cells* **133** 119–25

[90] Grenet L, Suzon M A A, Emieux F and Roux F 2018 Analysis of failure modes in kesterite solar cells *ACS Appl. Energy Mater.* **1** 2103–13

[91] Repins I L *et al* 2013 Indications of short minority-carrier lifetime in kesterite solar cells *J. Appl. Phys.* **114** 084507

[92] Maiberg M, Hölscher T, Jarzembowski E, Hartnauer S, Zahedi-Azad S, Fränzel W and Scheer R 2017 Verification of minority carrier traps in $Cu(In, Ga)Se_2$ and $Cu_2ZnSnSe_4$ by means of time-resolved photoluminescence *Thin Solid Films* **633** 208–12

[93] Hempel H, Hages C J, Eichberger R, Repins I and Unold T 2018 Minority and majority charge carrier mobility in $Cu_2ZnSnSe_4$ revealed by terahertz spectroscopy *Sci. Rep.* **8** 14476

[94] Park J S, Kim S, Xie Z and Walsh A 2018 Point defect engineering in thin-film solar cells *Nat. Rev. Mater.* **3** 194–210

[95] Kim S, Park J-S, Hood S N and Walsh A 2019 Lone-pair effect on carrier capture in Cu_2ZnSnS_4 solar cells *J. Mater. Chem.* A **7** 2686–93

[96] Wei Z, Fung C M, Pockett A, Dunlop T O, McGettrick J D, Heard P J, Guy O J, Carnie M J, Sullivan J H and Watson T M 2018 Engineering of a Mo/Si_xN_y diffusion barrier to reduce the formation of MoS_2 in Cu_2ZnSnS_4 thin film solar cells *ACS Appl. Energy Mater.* **1** 2749–57

[97] Kim S, Park J S and Walsh A 2018 Identification of killer defects in kesterite thin-film solar cells *ACS Energy Lett.* **3** 496–500

[98] López-Mir L, Galceran R, Herrero-Martín J, Bozzo B, Cisneros-Fernández J, Pannunzio Miner E V, Pomar A, Balcells L, Martínez B and Frontera C 2017 Magnetic anisotropy and valence states in $La_2Co_{1-x}Mn_{1+x}O_6$ ($x \approx 0.23$) thin films studied by x-ray absorption spectroscopy techniques *Phys. Rev.* B **95** 224434

[99] Maiberg M, Hölscher T, Zahedi-Azad S and Scheer R 2015 Theoretical study of time-resolved luminescence in semiconductors. III. Trap states in the band gap *J. Appl. Phys.* **118** 105701

[100] Ahrenkiel R K 1993 Minority-Carrier lifetime in III–V semiconductors *Semiconductors and Semimetals* ch 2 (Amsterdam : Elsevier) pp 39–150

[101] Mitzi D B, Gunawan O, Todorov T K, Wang K and Guha S 2011 The path towards a high-performance solution-processed kesterite solar cell *Sol. Energy Mater. Sol. Cells* **95** 1421–36

[102] 't Hooft G W and van Opdorp C 1986 Determination of bulk minority-carrier lifetime and surface/interface recombination velocity from photoluminescence decay of a semi-infinite semiconductor slab *J. Appl. Phys.* **60** 1065–70

[103] Kuciauskas D, Repins I, Kanevce A, Li J V, Dippo P and Beall C L 2015 Time-resolved recombination analysis in kesterite polycrystalline thin films and photovoltaic devices with one-photon and two-photon excitation *Sol. Energy Mater. Sol. Cells* **136** 100–5

[104] Redinger A and Unold T 2018 High surface recombination velocity limits Quasi-Fermi level splitting in kesterite absorbers *Sci. Rep.* **8** 1874

[105] Courel M, Andrade-Arvizu J A and Vigil-Galán O 2016 The role of buffer/kesterite interface recombination and minority carrier lifetime on kesterite thin film solar cells *Mater. Res. Express* **3** 095501

[106] Wang W, Winkler M T, Gunawan O, Gokmen T, Todorov T K, Zhu Y and Mitzi D B 2014 Device characteristics of CZTSSe thin-film solar cells with 12.6% efficiency *Adv. Energy Mater.* **4** 1301465

[107] Just J, Nichterwitz M, Lützenkirchen-Hecht D, Frahm R and Unold T 2016 Compositional dependence of charge carrier transport in kesterite Cu_2ZnSnS_4 solar cells *J. Appl. Phys.* **120** 225703

[108] Just J, Sutter-Fella C M, Lützenkirchen-Hecht D, Frahm R, Schorr S and Unold T 2016 Secondary phases and their influence on the composition of the kesterite phase in CZTS and CZTSe thin films *Phys. Chem. Chem. Phys.* **18** 15988–94

[109] Rudmann D, Brémaud D, Zogg H and Tiwari A N 2005 Na incorporation into $Cu(In,Ga)Se_2$ for high-efficiency flexible solar cells on polymer foils *J. Appl. Phys.* **97** 084903

[110] Caballero R, Kaufmann C A, Eisenbarth T, Cancela M, Hesse R, Unold T, Eicke A, Klenk R and Schock H W 2009 The influence of Na on low temperature growth of CIGS thin film solar cells on polyimide substrates *Thin Solid Films* **517** 2187–90

[111] Nagaoka A, Miyake H, Taniyama T, Kakimoto K, Nose Y, Scarpulla M A and Yoshino K 2014 Effects of sodium on electrical properties in Cu_2ZnSnS_4 single crystal *Appl. Phys. Lett.* **104** 152101

[112] Tampo H, Kim K M, Kim S, Shibata H and Niki S 2017 Improvement of minority carrier lifetime and conversion efficiency by Na incorporation in $Cu_2ZnSnSe_4$ solar cells *J. Appl. Phys.* **122** 023106

[113] Nagaoka A, Yoshino K, Taniguchi H, Taniyama T, Kakimoto K and Miyake H 2014 Growth and characterization of $Cu_2ZnSn(S_xSe_{1-x})_4$ alloys grown by the melting method *J. Cryst. Growth* **386** 204–7

[114] Gunawan O *et al* 2018 Carrier-resolved photo hall measurement in world-record-quality perovskite and kesterite solar absorbers arXiv:1802.07910

[115] Gunawan O, Virgus Y and Tai K F 2015 A parallel dipole line system *Appl. Phys. Lett.* **106** 062407

[116] Tai K F, Gunawan O, Kuwahara M, Chen S, Mhaisalkar S G, Huan C H A and Mitzi D B 2016 Fill factor losses in $Cu_2ZnSn(S_xSe_{1-x})_4$ solar cells: insights from physical and electrical characterization of devices and exfoliated films *Adv. Energy Mater.* **6** 1501609

[117] Guglietta G W, Choudhury K R, Caspar J V and Baxter J B 2014 Employing time-resolved terahertz spectroscopy to analyze carrier dynamics in thin-film $Cu_2ZnSn(S,Se)_4$ absorber layers *Appl. Phys. Lett.* **104** 253901

[118] Hempel H, Redinger A, Repins I, Moisan C, Larramona G, Dennler G, Handwerg M, Fischer S F, Eichberger R and Unold T 2016 Intragrain charge transport in kesterite thin films—limits arising from carrier localization *J. Appl. Phys.* **120** 175302

[119] Hempel H, Unold T and Eichberger R 2017 Measurement of charge carrier mobilities in thin films on metal substrates by reflection time resolved terahertz spectroscopy *Opt. Express* **25** 17227

[120] Hempel H, Eichberger R, Repins I and Unold T 2018 The effect of Cu-Zn disorder on charge carrier mobility and lifetime in $Cu_2ZnSnSe_4$ *Thin Solid Films* **666** 40–3

[121] Gokmen T, Gunawan O and Mitzi D B 2013 Minority carrier diffusion length extraction in $Cu_2ZnSn(Se, S)_4$ solar cells *J. Appl. Phys.* **114** 114511